J. Astrophys. Astr. (1987) **8**, 369–387

Spectroscopic Evolution of Nova LW Serpentis 1978 during its Early Decline

T. P. Prabhu & G. C. Anupama *Indian Institute of Astrophysics, Bangalore 560034*

Received 1987 May 28; accepted 1987 November 12

Abstract. Optical spectroscopic data are presented on nova LW Serpentis 1978, obtained during its decline from $V \simeq 9.0$ to $\simeq 10.2$ (compared to a value of ~ 8.0 at recorded maximum). The spectrum and its evolution compare well with a typical nova, though the principal absorption (~ -750 km s^{-1}) was very weak in comparison with the diffuse-enhanced absorption (~ -1300 km s^{-1}). The principal absorption could be identified only in the lines of O I $\lambda\lambda$7774, 8446, and in moderate-resolution observations of Hα. The salient features of spectral evolution follow: The near-infrared triplet of Ca II continuously weakened. O I λ8446 was always brighter than O I λ7774, indicating continued importance of Lyman β fluorescence. The lines due to [O I], [N II] and N II brightened considerably near the end of our observations (37 days from maximum). The Hα emission line was asymmetric all through with more emission towards the red. Its emission profile showed considerable structure. Based on the individual peaks in the Hα line profile, a kinematical model is proposed for the shell of LW Ser. The model consists of an equatorial ring, and a polar cone on the side away from the earth. The nearer polar cone did not show significant emission of Hα during our observations. The polar axis of the shell is inclined at a small angle ($\sim 15°$) to the line of sight.

Key words: stars, variable—stars, novae—spectroscopy, optical—stars, individual

1. Introduction

Nova LW Serpentis was discovered by Honda (1978) on 1978 March 1 at a photographic magnitude of 9.0. The nova was well-observed in the infrared band, and is one of the few novae in which the formation of optically thick dust shells has been well-studied (Szkody *et al.* 1979; Gehrz *et al.* 1980). On the other hand, the optical light curve was not monitored well except as visual estimates. The maximum recorded brightness was $m_{pg} = 8.3$ on March 4 (Kozai 1978). The available *UBV* data has been compiled by van den Bergh & Younger (1987).

The nature of the light curve places LW Ser among class II novae (in the nomenclature of Duerbeck 1981), exhibiting structured (as against class I: smooth) light curve. Duerbeck ascribes it the type Cb, similar to nova FH Ser 1970. Nova NQ Vul 1976 (Bb) also had a similar light curve. All these novae had fairly deep minima in

the transition stage and exhibited well-developed dust shells. The development of the dust shell in LW Ser bore a striking resemblance to that of NQ Vul (Bode & Evans 1983).

The optical spectrum of LW Ser was briefly described by Herbig (1978), and Prabhu (1978). Herbig measured on March 13.5 UT an Hα absorption velocity of $-1500\,\mathrm{km\,s^{-1}}$, whereas Prabhu obtained a mean absorption velocity of $-1240\pm 60\,\mathrm{km\,s^{-1}}$ from several lines between March 10.92 and 11.97. On the other hand, Cohen & Rosenthal (1983) obtained an expansion velocity of $\sim 600\,\mathrm{km\,s^{-1}}$ a few years later, based on the widths of emission lines.

LW Ser was monitored spectroscopically at the Vainu Bappu Observatory (VBO), Kavalur, for nearly a month following its maximum. A preliminary description of the spectrum was given recently by Prabhu & Anupama (1987). Detailed results are presented here together with the Hα profiles obtained at moderate resolution. A qualitative kinematical model of the shell is also constructed based on the structure of Hα profile.

2. Observations and reductions

Several spectra were recorded between 1978 March 10 and April 7 using the 1-m reflector and the Cassegrain spectrograph equipped with a Varo 8605 single-stage image intensifier at VBO. A set of gratings (80, 300, and $600\,\mathrm{g\,mm^{-1}}$) were used in conjunction with a camera of focal length 175 mm, yielding reciprocal dispersions of 675, 166, and $83\,\mathrm{Å\,mm^{-1}}$ in the wavelength range of 3900–8800 $\mathrm{Å\,mm^{-1}}$. Occasionally, the Hα line was observed at $30\,\mathrm{Å\,mm^{-1}}$ using a grating of $1800\,\mathrm{g\,mm^{-1}}$. The journal of observations appears in Table 1.

Table 1. Journal of observations.

1978 UT		Exposure min	Wavelength range Å	Dispersion $\mathrm{Å\,mm^{-1}}$
March	10.90	5	4600–8800	675
	10.92	23	4000–8800	166
	10.94	10	4000–8800	166
	10.96	10	Hα	30
	11.00	16	3900–6700	166
	11.01	16	3900–6700	166
	11.91	60	7000–8800	83
	11.97	60	7000–8800	83
	12.00	20	4900–7300	83
	25.90	45	Hα	30
	27.88	50	Hα	30
	27.94	72	7000–8800	83
	31.89	53	Hα	30
April	2.91	69	Hα	30
	6.94	6	4600–8700	675
	7.94	10	4600–8700	675

The spectra were recorded on Kodak IIa-D (except on one occasion when it was Kodak 103a-D) held in contact with the output fibre-optic face-plate of the image intensifier. All the spectra were calibrated to relative intensity scale using an auxiliary calibration spectrograph equipped with a rotating sector to yield 11 one-mm steps at relative exposure intervals of $\Delta \log E = 0.1$. No spectrophotometric standard star was observed, and hence no attempt is made to correct the spectra for instrumental response.

The spectrograms were digitized at 5 μm intervals using a 10 μm wide aperture on the PDS 1010M microdensitometer at the Indian Institute of Astrophysics (IIA), Bangalore, and analyzed using the software RESPECT (Prabhu, Anupama & Giridhar 1987), mostly at the VAX 11/780 system at VBO. Not all the spectrograms listed in Table 1 were digitized: A choice was made based on exposure and dispersion. Some of the spectrograms were measured on the Abbé comparator in order to derive absorption velocities.

3. The spectrum and its evolution

Observations with good spectral coverage were obtained only on three epochs: (1) on the nights of March 10–12 about 10 days after maximum, when LW Ser was at $V \simeq 9.0$ ($\lambda\lambda$3900–8800); (2) on March 27 at $V \simeq 9.5$ ($\lambda\lambda$7000–8800); and (3) on April 6–7 at $V \simeq 10.2$ ($\lambda\lambda$4600–8700). The Hα profile was recorded at better resolutions once on March 10, and four times between March 25 and April 2. We discuss in this section the nature and evolution of the spectrum at these epochs.

3.1 *The Line Identification and Equivalent Widths*

The emission lines in LW Ser were identified using the catalogue of Meinel, Aveni & Stockton (1975), and also by comparing with the spectra of some novae published in the literature. The large widths of emission lines (FWHM ~ 1200 km s^{-1}) and the consequent line-blending made the line identification a fairly difficult task, particularly shortward of Hα. Hence, whenever at least one bright line of a multiplet could be unambiguously identified, we have assumed the multiplet to be present. On April 6 and 7, we could record spectra only at low dispersions. The identification of lines in these spectra were carried out through a comparison with detailed spectra at earlier epochs.

The spectra reduced to continua are shown in Figs 1 and 2. The continuum was slightly underexposed on March 27, and considerably so on April 7. The line identifications and emission-line equivalent widths are listed in Tables 2a and b. The equivalent widths are rather uncertain when continua are underexposed. However, they illustrate the general trend in the evolution of the spectrum. Comments on individual elements follow.

Hydrogen: The Balmer series of hydrogen could be identified clearly only at Hα, Hβ, and Hγ in our spectra. Hδ and Hε could be identified on the spectra recorded during March 10–12. Both these lines had blends towards longer wavelengths. Ti II (11) is a likely contributor to Hε, whereas Si II (3) is possibly present in the red wing of Hδ. The

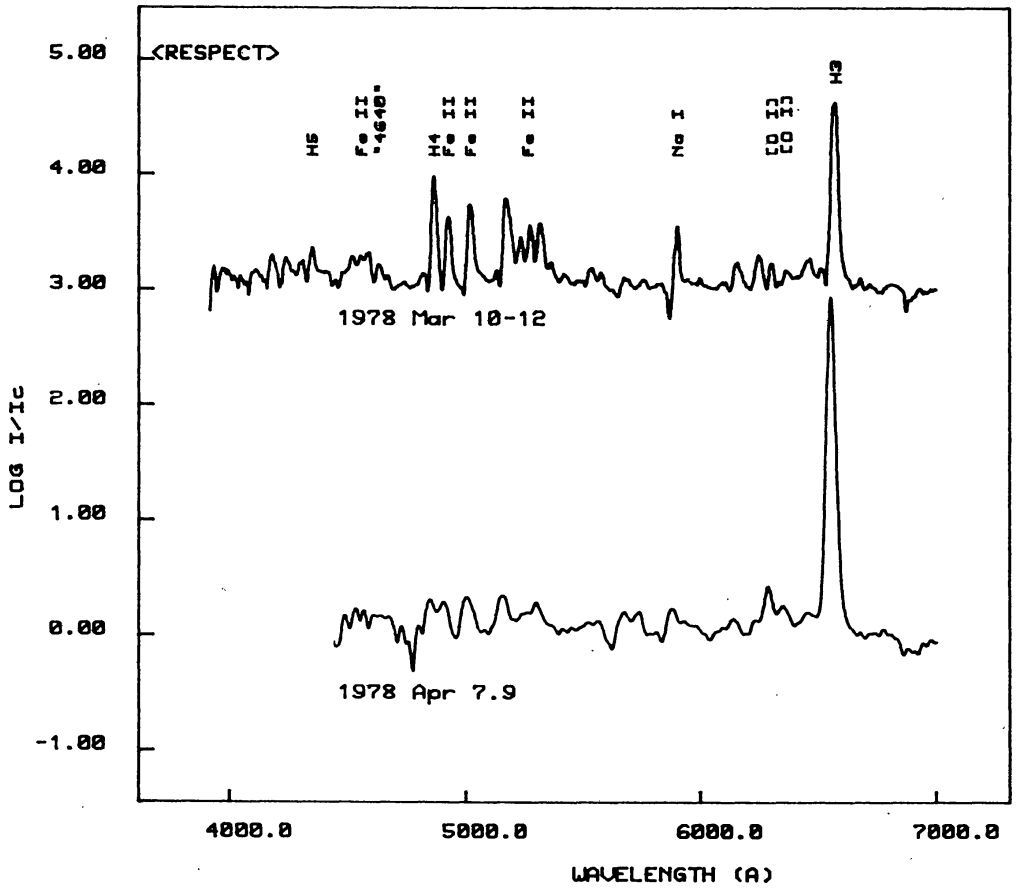

Figure 1. Spectra of LW Ser in the range $\lambda\lambda$3900–7000 on 1978 March 10–12 and April 7, reduced to the continuum intensity. A bias of 3 has been added to the $\log(I/I_c)$ scale for the earlier spectrum.

presence of Ca II K near the edge of the recorded spectrum suggests that Ca II H contributed to Hε.

Carbon: C II $\lambda\lambda$7231, 7236 (multiplet 3) and $\lambda\lambda$7112–7119 (20) were the only lines of carbon easily seen in our spectra. The line at λ7236 appears to have increased in brightness with time. However, this line is blended with O I (20). Though there is some suggestion of C I λ8335(1) in Fig. 2, the spectrum is considerably underexposed in that region to enable definite identification.

Nitrogen: N I $\lambda\lambda$8680–8728(1) feature was blended with Ca II λ8662, whereas N I $\lambda\lambda$8184–8242(2) was clearly present, though affected by atmospheric absorption and blended with O I (34). The multiplet 3 at $\lambda\lambda$7423–7468 was blended with Fe II (73) and O I (55). The lines at $\lambda\lambda$8594, 8629 (8) were blended with the wings of Ca II $\lambda\lambda$8542, 8662. The brighter of these (λ8629) was superposed over the P Cygni absorption of λ8662. The "4640" complex of O II (1), N II (5), N III (2) appeared flat-topped around April 7, on a rather underexposed spectrogram.

The best-seen lines of N II were $\lambda\lambda$5452–5495 (2), $\lambda\lambda$5666–5710 (3), and $\lambda\lambda$5931–5952 (28). [N II] λ5755 (3) could also be identified all through.

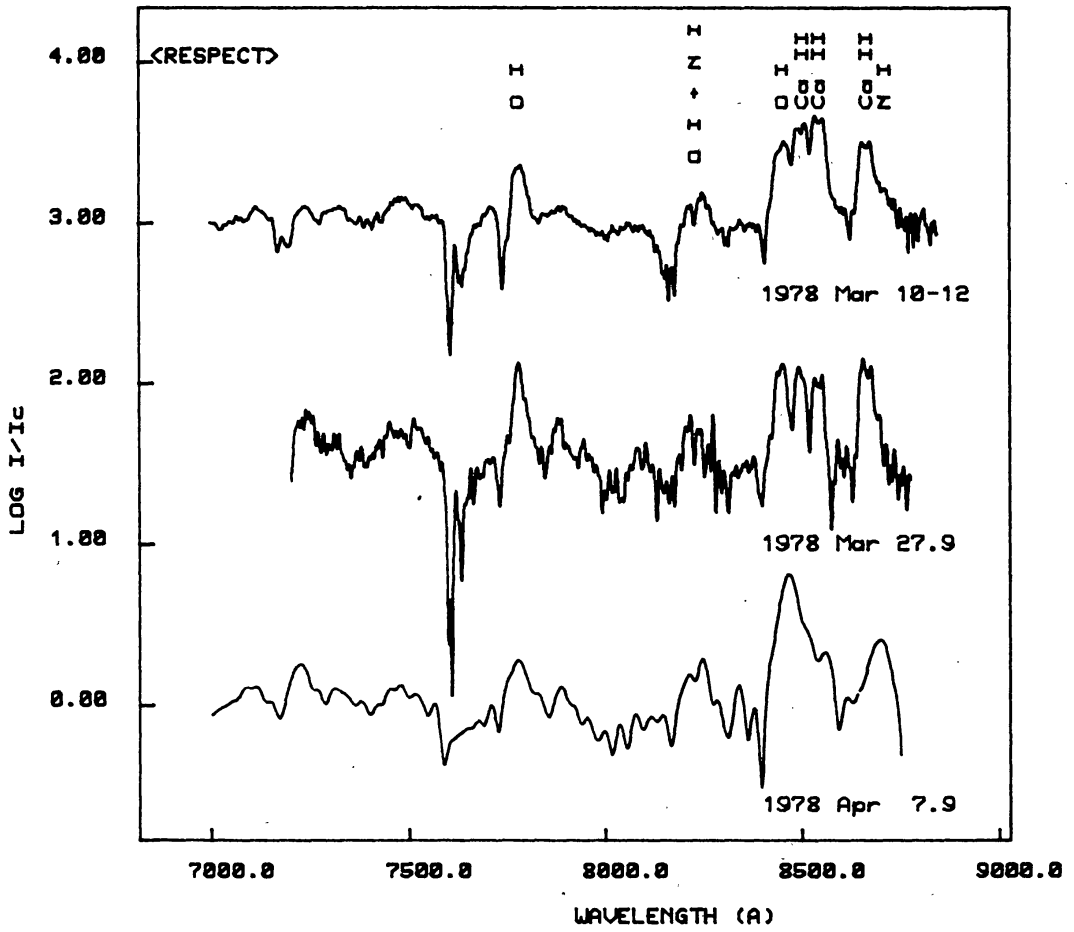

Figure 2. Spectra of LW Ser in the range $\lambda\lambda$7000–8800 on 1978 March 10–12, March 27 and April 7, reduced to the continuum intensity. Bias of 3 and 1.5 have been added to the $\log(I/I_c)$ scale for the first and second spectrum, respectively.

Table 2a. Line identifications and emission equivalent widths in the visual region.

Measured wavelength	Identification	Equivalent width (Å) March 10–12 (day 10)	April 7 (day 37)
3934	3933.66 Ca II K (1)	8	
3971	3968.47 Ca II H (1) 3970.07 Hε		
	4012.37 Ti II (11)* 4025.14 Ti II (11)* 4028.33 Ti II (87)*	27	
4056	4053.81 Ti II (87) 4056.21 Ti II (11)	7	
4108	4101.74 Hδ 4128.05 Si II (3)* 4130.88 Si II (3)* 4097.31 N III (1)* 4103.37 N III (1)*	23	

Table 2a. Continued.

Measured wavelength	Identification	Equivalent width (Å) March 10–12 (day 10)	Equivalent width (Å) April 7 (day 37)
4180	4178.86 Fe II (28) 4173.45 Fe(27)† 4177.70 Fe II (21)† 4185.46 O II (36)* 4189.79 O II (36)*	31	
4240	4233.17 Fe II (27) 4236.93 N II (48) 4237.05 N II (48) 4241.79 N II (48)	27	
4269:	4258.16 Fe II (28)* 4258.35 Fe II (21)* 4273.32 Fe II (27)*	8	
4300	4296.57 Fe II (28) 4303.17 Fe II (27)	23	
4351	4340.47 Hγ 4351.76 Fe II (27)	36	
4413:	4385.38 Fe II (27)* 4416.82 Fe II (27)* 4395.03 Ti II (19)* 4417.12 Ti II (40)*	22	
4446	4443.80 Ti II (19) 4447.03 N II (15)	4	
4478	4481.13 Mg II (4) 4481.33 Mg II (4)	14	
4520	4515.34 Fe II (37) 4520.23 Fe II (37) 4522.63 Fe II (38) 4501.27 Ti II (31)*	26	47
4556	4549.76 Fe II (38) 4555.89 Fe II (37) 4533.97 Ti II (50)* 4549.62 Ti II (82)* 4563.76 Ti II (50)* 4571.97 Ti II (82)*	25	
4587	4582.84 Fe II (37) 4583.83 Fe II (38) 4595.68 Fe II (38)	32	
4636	4629.34 Fe II (37) "4640" CNO Complex	19	44
4670	4666.75 Fe II (37) 4698.5 O II (40)	6	
4730	4731.44 Fe II (43) 4708.66 Ti II (49)*	6	2
4817	4825.71 Fe II (30) 4805.11 Ti II (92)*	14	3

Table 2a. Continued.

Measured wavelength	Identification	Equivalent width (Å) March 10–12 (day 10)	Equivalent width (Å) April 7 (day 37)
4866	4861.33 Hβ	180	45
4926	4923.92 Fe II (42)	83	44
5018	5018.43 Fe II (42)	132	65
5132	5129.14 Ti II (86)	11	
5174	5169.03 Fe II (42) 5175.89 N II (66) 5179.50 N II (66) 5185.90 Ti II (86)* 5197.57 Fe II (49)*	178	71
5236	5234.62 Fe II (49)	52	
5281	5275.99 Fe II (49) 5284.09 Fe II (41) 5264.80 Fe II (48)‡	69	
5319	5316.61 Fe II (49) 5325.56 Fe II (49)‡ 5316.78 Fe II (48)‡ 5336.81 Ti II (69)*	86	88
5365	5362.86 Fe II (48) 5381.02 Ti II (69)*	23	
5423	5414.09 Fe II (48) 5425.27 Fe II (49)† 5432.98 Fe II (55)	14	
5481	5452.12 N II (29) 5454.26 N II (29) 5462.62 N II (29) 5478.13 N II (29) 5480.10 N II (29) 5495.70 N II (29)	10	24
5539	5534.86 Fe II (55) 5530.27 N II (63) 5535.39 N II (63)	19	
5581	5577.35 [O I] (3)	11	14
5685	5666.64 N II (3) 5676.02 N II (3) 5679.56 N II (3) 5710.76 N II (3)	10	27
5755	5754.80 [N II] (3)	8	26
5823	5824.40 Fe II (58)	5	2
5901	5889.95 Na I (1) 5895.92 Na I (1)	52	33
5945:	5931.79 N II (28) 5940.25 N II (28) 5941.67 N II (28) 5952.39 N II (28)	8	21
5989:	5991.38 Fe II (46)	8	

Table 2a. Continued.

Measured wavelength	Identification	Equivalent width (Å) March 10–12 (day 10)	April 7 (day 37)
6100	6084.11 Fe II (46) 6113.33 Fe II (46)	6	7
6157	6147.74 Fe II (74) 6149.24 Fe II (74) 6155.99 O I (10) 6156.78 O I (10) 6158.19 O I (10) 6185.34 Fe II (46)*	27	18
6250	6247.56 Fe II (74) 6242.52 N II (57)†	34	9
6302	6300.23 [O I] (1)	16	71
6334	—	3	
6366	6363.88 [O I] (1) 6369.45 Fe II (40) 6379.63 N II (2)* 6347.09 Si II (2)* 6371.36 Si II (2)*	16	45
6400:	6407.30 Fe II (74)* 6416.91 Fe II (40)*	7	
6460	6456.38 Fe II (74) 6453.64 O I (9) 6456.01 O I (9) 6432.65 Fe II (40)* 6482.07 N II (8)*	44	39
6511	6516.05 Fe II (40) 6504.9 N II (45)*	14	
6568	6562.82 Hα	1074	over-exposed
6673	6678.15 He I	6	
6719		3	
6811		6	

* Blended with the neighbouring feature.
† Minor contributor to the feature.
Multiplet numbers appear in parantheses.

The lines of nitrogen increased in strength by a factor of 3–4 with respect to the continuum, between March 10 and April 7.

Oxygen: The most prominent at all stages of the spectrum were O I λ8446 (4), enhanced by Lyman β fluorescence, and O I λ7774 (1). A few other lines of O I were also seen: λ6454 (9), λ6157 (10) as blends with Fe II; λλ7982–7995 (19) and λλ7947–7952 (35) blended with each other. O I (20) probably contributed to C II (3). The lines at λλ7476–7480 (55) were present, blended with the lines of Fe II and N I. The forbidden lines [O I] λλ6300, 6364 (1) and λ5577 (3) were seen more easily and

Table 2b. Line identifications and emission equivalent widths in the near-infrared region.

Measured wavelength	Identification	Equivalent width (Å) March 10–12 (day 10)	March 27 (day 26)	April 7 (day 37)
7116	7112.36 C II (20) 7115.13 C II (20) 7119.45 C II (20)	9		19
7236	7224.51 Fe II (73) 7231.12 C II (3) 7236.19 C II (3) 7254.19 O I (20) 7254.47 O I (20)	10	46	43
7314	7289.05 Fe II (72) 7301.57 Fe II (72) 7307.97 Fe II (73) 7310.24 Fe II (73) 7320.70 Fe II (73) 7291.46 [Ca II] (1) 7323.88 [Ca II] (1)	14	23	12
7423	7423.63 N I (3)	1	6	
7479	7442.28 N I (3) 7468.29 N I (3) 7476.45 O I (55) 7479.06 O I (55) 7480.66 O I (55) 7462.38 Fe II (73) 7515.88 Fe II (73) 7479.70 Fe II (72) 7533.42 Fe II (72)	32	69	20
7707	7711.71 Fe II (73)	7	under-exposed	
7782	7771.90 O I (1) 7774.18 O I (1) 7775.40 O I (1)	47	107	44
7882	7877.13 Mg II (8) 7896.37 Mg II (8) 7841.40 Fe II (72)*	14	30	8
7950	7947.56 O I (35) 7950.83 O I (35) 7952.18 O I (35) 7982.41 O I (19) 7987.00 O I (19) 7995.12 O I (19)		6	
8215 + 8249	8184.80 N I (2) 8187.95 N I (2) 8216.28 N I (2) 8223.07 N I (2) 8242.34 N I (2) 8221.84 O I (34) 8227.64 O I (34) 8230.01 O I (34) 8232.99 O I (34)	18:	28:	43:

Table 2b. Continued.

Measured wavelength	Identification	Equivalent width (Å) March 10–12 (day 10)	March 27 (day 26)	April 7 (day 37)
8338	8335.19 C I (10)			5:
8448	8446.35 O I (4)			
	8446.76 O I (4)	86:	110	
	8437.96 HP_{18}†			356
	8467.26 HP_{17}†			
8499	8498.02 Ca II (2)			
	8502.49 HP_{16}†	119:	85	
8544	8542.09 Ca II (2)		75	
	8545.38 HP_{15}†	149:		
8603:	8594.01 N I (8)		4:	
	8598.39 HP_{14}†			
8666	8662.14 Ca II (2)			
	8665.02 HP_{13}†	90		
	8629.24 N I (8)*			91
8711:	8680.24 N I (1)		130	
	8683.38 N I (1)			
	8686.13 N I (1)			
	8703.24 N I (1)	24		
	8711.69 N I (1)			
	8718.82 N I (1)			
	8728.88 N I (1)			
8810	8806.77 Mg I (7)	2:		

* Blended with the neighbouring feature.
† Minor contributor to the feature.
Multiplet numbers appear in parantheses.

appeared fairly strong on April 7. Si II (2), N II (2) and Fe II (40) were blended with [O I] (1) during the first epoch. N II (2) increased its contribution whereas the other blends weakened with time. O I λ8446 strengthened dramatically between March 10 and April 7.

Magnesium: The emissions at λλ4478 and 7881 are possibly due to Mg I λ4481 (4), and λλ7877, 7896 (8). Multiplet 7 (λ8806) was also possibly present. The lines due to Mg I have been identified in several novae (Andrillat & Houziaux 1987).

Sodium: Na I D λλ5890, 5896 (1) were fairly bright all through the spectral evolution.

Silicon: The only identifiable lines of Si were Si II λλ4128, 4130 (3) blended with Hδ and λλ6347, 6371 (20) blended with [O I] (1).

Calcium: The near-infrared triplet of Ca II λλ8498, 8542, 8662 (2) was very bright on March 10–12, but faded considerably by April 6–7. H and K lines (1) were also seen in

the early spectrum. [Ca II] $\lambda\lambda$7291, 7323 (1) were possibly present during the later epochs.

Titanium: It is possible that several lines of Ti II were present; the only relatively unblended features were however λ4053 (87) + λ4056 (11), and λ5129 (86).

Iron: Lines of Fe II were particularly strong in the early spectrum, but faded with time. Strongest among these were multiplets 42, 48 and 49. Clearly visible were also multiplets 27, 28, 37, 38, 40, 46, 73 and 74.

3.2 *The Velocities*

Absorption velocities could be derived from comparator measurements at only one epoch (March 10–11 $\simeq$ day 10). The derived velocities are listed in Table 3 together with a few values derived from the digitized data. The most conspicuous absorption system is identified with the diffuse-enhanced spectrum. The decreasing magnitude of this velocity with increasing quantum number for the Balmer lines is a phenomenon well-observed in novae. The comparator measurements of Fe II, Na I D, and O I λ7774 lines yield a mean absorption velocity of -1300 ± 60 km s^{-1}. This value agrees with the older, independent, measurements of the same plates, which gave a value of -1240 ± 60 km s^{-1} (Prabhu 1978).

The line profiles of O I $\lambda\lambda$7774, 8446 show weak absorption at -820 km s^{-1} (March 10–12), and -690 km s^{-1} (March 27). The Hα line profiles obtained at moderate resolution show similar absorption features around -700 km s^{-1} (March 10–25). These absorptions are identified with the principal velocity system. The Hα

Table 3. Absorption line velocities.

	Absorption velocity (km s^{-1})		
Emission line	March 10–12 (day 10)	March 27 (day 26)	April 7 (day 37)
4101 Hδ	(−1460:)		
4340 Hγ	−870		
4629 Fe II (37)	−1270		
4861 Hβ	−1319		
4924 Fe II (42)	−1401		
5018 Fe II (42)	(−1416)		
5169 Fe II (42)	−1281		
5893 Na I (1)	−1265		
6563 Hα	−1482		(−1770)*
	(−700)	(−700)	(−760)*
7774 O I (1)	−1279	(−1620)	(−1770)
	(−813)	(−662)	
8446 O I (4)	(−1395)	(−1646)	(−1797)
	(−830)	(−769)	
8662 Ca II (2)	(−1330)		

The values in parantheses were measured on the digitized spectra.
* On April 2.

line also showed an absorption at ~ -1770 km s^{-1} on April 2, whereas the lines of O I $\lambda\lambda$7774, 8446 showed absorption at similar velocities on April 7. These may be ascribed to the Orion absorption system.

The absorption systems seen in LW Ser are in accordance with those observed in novae of moderate speed class (Gallagher & Starrfield 1978). However, the principal absorption system was rather weak in LW Ser.

3.3 *The Hα Line-Profile*

The Hα profiles on March 11, 25, 27 and April 2 are shown in Fig. 3, reduced to the continuum intensity, based on spectrograms obtained at 30 Å mm^{-1}. The continuum was not generally well-exposed. The absorption at -1480 km s^{-1} is barely visible on March 11. The profile of April 2 shows a shallow and broad absorption feature ~ -1770 km s^{-1}. The principal absorption is also visible.

At a very first glance the Hα profile is seen to be asymmetric with more emission towards the red. The centre of the profile lies at 300 km s^{-1}, an unlikely velocity for

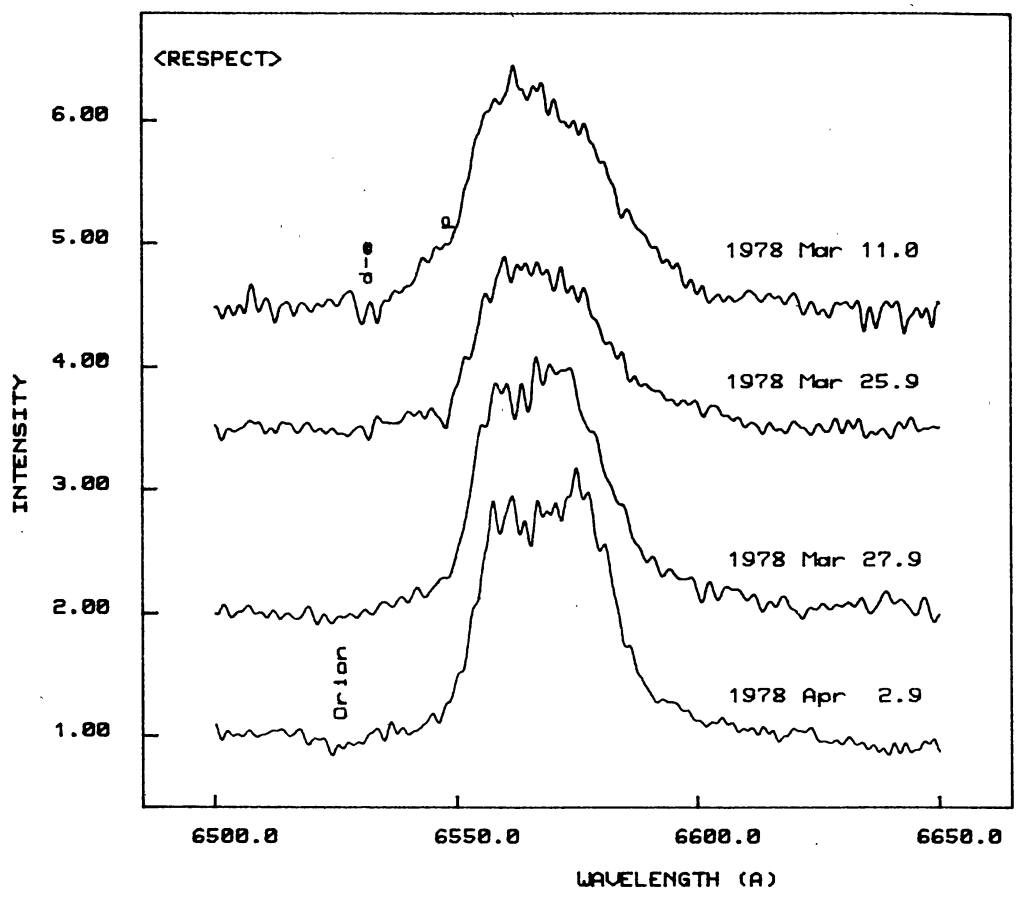

Figure 3. The line profiles of Hα between 1978 March 11 and April 2, reduced to the continuum intensity. The principal (p), diffuse-enhanced (d-e), and the Orion absorptions have been marked. Bias of 3.5, 2.5 and 1 have been added to the respective intensities of the first three spectra.

the system. Though the profile is very nearly flat-topped, some structure is evident near the peak, particularly after March 25.

It is likely that [N II] λλ6548, 6584 contribute to the emission at Hα. In order to estimate their contribution, the profiles of Hα and [N II] were assumed to be similar, and a de-blending procedure in RESPECT was used. Fig. 4 shows the mean of observed profiles in intensity units, with the contributions due to Hα and [N II] shown separately. A ratio of 3 was assumed for [N II] λ6584/λ6548. The halfwidth of Hα line is now reduced to 1200 km s^{-1}. The asymmetry of the profile persists, though reduced in magnitude. The Hα/[N II] ratio of about 6 gives the best fit determined interactively.

More discussion on the Hα line profile appears in Section 4 where a qualitative, kinematical model is attempted.

3.4 *Comparison with other Novae*

McLaughlin (1960, and references therein) describes the spectral evolution of a 'typical' nova, with respect to the position on the light curve both in terms of

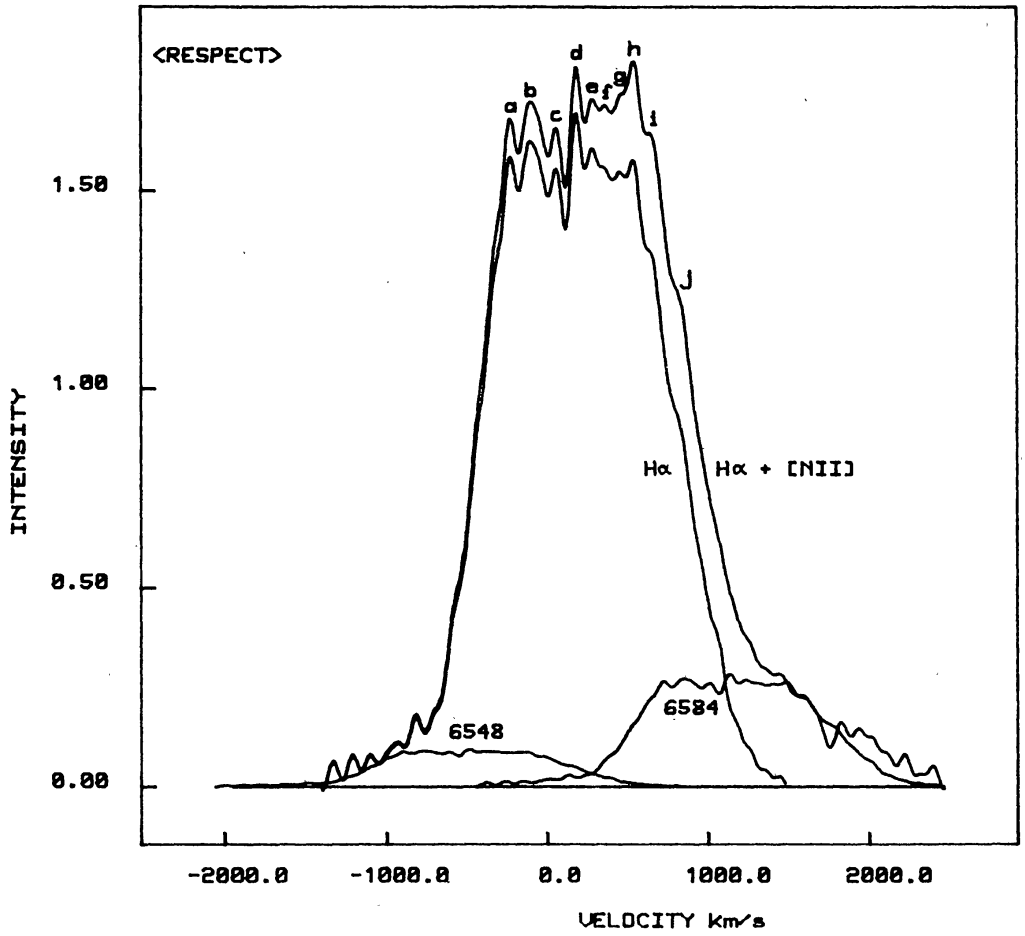

Figure 4. Mean Hα profile between 1978 March 25 and April 2. The contributions due to [N II] λ6548, Hα, and [N II] λ6584 have been separated out. The velocity scale refers to Hα. Peaks referred to in the text and Table 4 have been marked a–j.

magnitudes from the maximum, and with respect to a scaled time coordinate. One may compare the evolution of LW Ser with that of a typical nova, and also with other novae that exhibited a similar light curve—DQ Her (Stratton & Manning 1939), FH Ser (Andersen, Borra & Dubas 1971), and NQ Vul (Yamashita *et al.* 1977; Shcherbakov 1977; also unpublished VBO spectra).

The discovery magnitude of $m_{pg}=9$ on 1978 March 1 UT, and the value of $m_{pg}=8.3$ on March 4.82 UT suggest that LW Ser reached its maximum between March 1 and 4. If we assume $m_{pg}=8.3$ at the maximum and a colour index of 0.35 at this stage (Duerbeck 1981), we arrive at a visual magnitude of ~ 8.0. The three epochs of observation would then correspond to 1.0, 1.5 and 2.2 mag below maximum. For a typical nova spectrum, these stages would correspond approximately to (1) the principal spectrum, (2) advanced stages of the diffuse-enhanced spectrum, and (3) Orion absorption stage close to the onset of [O I] flash.

McLaughlin (1960) also describes evolution as a function of time expressed in the units of t_3, the time required to decline by three visual magnitudes. Duerbeck (1981) lists $t_3=50$ d for LW Ser. Assuming the zero of time to be March 1.5 (Gehrz *et al.* 1980), we obtain for the three epochs: (1) 10 days after maximum the diffuse-enhanced absorption would have just appeared; (2) 26 days after maximum, the nova was past the maximum of diffuse-enhanced phase, and the Orion absorption would have just appeared; (3) 37 days after maximum [O I] flash had just occurred.

The evolution of spectrum of LW Ser agrees generally with other novae of similar speed class. The major difference is in the weakness of the principal absorption in LW Ser and the early appearance and strength of diffuse-enhanced spectrum, if our identification of velocity systems is correct. The difference is particularly striking in comparison with NQ Vul, in which case the principal absorption was very strong.

4. Geometrical structure of the shell

High-resolution imaging and spectroscopy of shells around old novae indicate that a typical nova shell consists of an equatorial ring and a pair of polar caps. Particular examples are DQ Her and V603 Aql (Mustel & Boyarchuk 1970; Weaver 1974), and HR Del (Solf 1983). It also appears that these components are confined within a prolate ellipsoidal shell, the expansion velocity being smaller at the equator than at the poles.

A typical nova shell thus appears to consist of rings of matter at different latitudes with respect to an axis of symmetry. If there is continuous ejection of matter, these rings take the shape of hollow cones with different angles of opening with respect to a common axis (Solf 1983). The polar cap can be considered as a cone with a small angle of opening. We will refer to these components as cones in the following for convenience and uniformity of terminology.

4.1 *General Considerations*

Emission profile due to an individual cone is generally double-peaked, and is sharply bounded by the velocities

$$V_{r,b}=V_0+V\cos(\phi\pm i) \qquad (1)$$

where V_r, V_b are red and blue limits of the profile, V_0 is the systemic velocity, ϕ the semi-angle of opening, i the inclination of the polar axis to the line of sight, and V the velocity of expansion of the cone. V can be expressed as

$$V=(V_p^2\cos^2\theta+V_e^2\sin^2\theta)^{1/2} \tag{2}$$

where V_p, V_e are polar and equatorial expansion velocities and θ the parametric angle given by

$$\tan\theta=\frac{V_p}{V_e}\tan\phi. \tag{3}$$

The cones are assumed to be embedded in a prolate ellipsoidal shell with the longer axis making an angle i with the line of sight. The section of the ellipsoid in the plane defined by the line of sight and the longer axis would be an ellipse. The expansion velocities along the perimeter of the ellipse can be parametrized by

$$V_x=V_p\cos\theta\cos i-V_e\sin\theta\sin i, \tag{4a}$$

$$V_y=V_p\cos\theta\sin i+V_e\sin\theta\cos i, \tag{4b}$$

where the x-axis is chosen along the line of sight. The maximum velocity component along the line of sight would then be given by V_x such that

$$\frac{dV_x}{d\theta}=0, \tag{5a}$$

whereas the absorption velocity would correspond to V_x at

$$V_y=0. \tag{5b}$$

Obtaining the corresponding values of θ, and substituting in Equation (4a), it can be derived that emission from the shell is contained within

$$V_{max}=V_p(\cos^2 i+f^2\sin^2 i)^{1/2}, \tag{6}$$

where $f=V_e/V_p$, and that the absorption component is at

$$V_{abs}=-\frac{V_e}{(f^2\cos^2 i+\sin^2 i)^{1/2}}. \tag{7}$$

Eliminating ϕ and θ from Equations (1)–(3) one obtains the conditions

$$(x-\delta)^2+y^2=1 \tag{8}$$

where $x=\frac{1}{2}(V_r+V_b)/V_p\cos i$, $y=\frac{1}{2}(V_r-V_b)/V_e\sin i$, and $\delta=V_0/V_p\cos i$. Thus, if the observed profile is separated into components corresponding to different cones, the values (x_i, y_i) lie on a unit circle with centre at $(\delta, 0)$. A least-squares fit can hence be obtained to derive optimal values of V_0, V_p, V_e and i. The values of ϕ can then be derived from

$$\tan\phi=\frac{fy}{x-\delta}. \tag{9}$$

4.2 *A Kinematical Model*

The fact that Hα profile showed structure on March 25 suggests that the shell had already broken into equatorial rings and polar cones. Since the material was still optically thick to line radiation it is difficult to model the line profile in terms of contributions due to individual cones. However, the velocities of peaks may be used to obtain a qualitative kinematical model following Section 4.1.

We use the averaged Hα profile so that the effect of residual noise is reduced in the identification of peaks. After correcting for [N II], the most prominent peaks in Hα profile were at velocities −240, −110, +50, +180, +270, and +530 km s^{-1}. There appeared fainter peaks at 360 and 460 km s^{-1}. There were several undulations on the red wing of Hα+[N II] profile. Prominent among these were at +640 and 840 km s^{-1}. All these features are marked a–j in Fig. 4.

Rms deviations of observed peaks from the circle given by Equation (8) were obtained for all possible combinations of pairs (V_r, V_b) chosen from among the prominent six peaks. The nature of scaling of Equation (8) is such that rms deviations for different sets of parameters can be compared only if we define the rms residual as

$$\langle(\Delta s)^2\rangle^{1/2} = \langle[(\Delta x\, V_p \cos i)^2 + (\Delta y\, V_e \sin i)^2]\rangle^{1/2}. \quad (10)$$

The residuals were computed for V_p ranging between 600 and 1600 km s^{-1}, i between 1° and 89°, and V_0 between −100 and +100 km s^{-1}. The value of f was fixed at 0.67 in analogy with the observed shell of DQ Her. The model with the least rms residual was chosen as the best model. An increase in the assumed value of f would decrease the derived value of inclination. An increase in the value of V_p would also have the same effect.

It was found that the residuals are sensitive to the choice of (V_r, V_b) pairs, but rather insensitive to the values of V_p. The best fit was obtained for pairs (−240, 50), (−110, 180), (270, 530) km s^{-1}. The rms residual was $\lesssim$20 km s^{-1} over the entire range of V_p.

The choice of V_p was made by constraining the model value of V_{abs} to the observed value of −750 km s^{-1}. The best fit model thus obtained is listed in Table 4. The model

Table 4. Model parameters for the shell of LW Ser.

		Model 1	Model 2
	V_p (km s^{-1})	800	1100
	f	0.67	0.67
	V_0 (km s^{-1})	40	−10
	i	16	11
	V_{max} (km s^{-1})	783	1089
	V_{abs} (km s^{-1})	−765	−1076
Identification in Fig. 4	Peak velocities (km s^{-1}) V_b	V_r	ϕ (deg)	
(a, c)	−240	50	101	98
(b, d)	−110	180	86	87
(e, h)	270	530	48	59

is clearly asymmetric, with no polar cone on the hemisphere facing the earth. The polar axis subtends a small angle (11°–16°) to the line of sight. Furthermore, two of the rings are equatorial and the third could be termed polar. The minor peaks can be attributed to structure in the polar cone.

The presence of significant emission at Hα beyond $\sim 800\ \mathrm{km\,s^{-1}}$ suggests that the value of V_p could be larger than this value. If the constraint on V_{abs} is removed—which is anyway based on a rather faint dip in the profile—one obtains the alternative model listed in Table 4 with $V_p = 1100\ \mathrm{km\,s^{-1}}$. The emission shortward of the dip $\sim -750\ \mathrm{km\,s^{-1}}$, as also the emission at $\gtrsim 800\ \mathrm{km\,s^{-1}}$, can then be ascribed to the polar regions. However, there would remain significant emission at $\phi \sim 60°$ with only weak emission at $\phi \sim -60°$.

5. Discussion

LW Ser belongs to a class of novae that exhibit a moderate rate of decline, and a transition phase associated with infrared emission due to an optically thick dust shell.

Using the absolute-magnitude–rate-of-decline relationship, Gehrz *et al.* (1980) obtained an absolute magnitude of $M_v = -7.2$ at the maximum of LW Ser. Assuming $A_v = 1.0$, and m_v (max) $\simeq 7.9$, they derived a distance of $D = 6.3$ kpc. Their infrared observations, however, yielded an angular diameter of 22.7 milli-arcsec 75 days from maximum, a value inconsistent with the above distance, and an assumed value of $1250\ \mathrm{km\,s^{-1}}$ for the velocity of expansion.

Van den Bergh & Younger (1987) derived mean values of $(B-V)_0 = -0.02 \pm 0.04$ and $M_v\,(15) = -5.23 \pm 0.16$ fifteen days after maximum for all but the fastest novae. The observed values of $(B-V)_0 = 0.50$ and $V = 9.5$ for LW Ser 15 days after estimated maximum (Gehrz *et al.* 1980) imply $E(B-V) = 0.52$, $A_v = 1.6$ and $D = 4.2 \pm 0.4$ kpc. This value is in fair agreement with the distance suggested by Gehrz *et al.* (1980) assuming a value of $1250\ \mathrm{km\,s^{-1}}$ for expansion velocity.

On the other hand, Cohen & Rosenthal (1983) used an expansion velocity $\sim 600\ \mathrm{km\,s^{-1}}$, which reduced the implied distance to LW Ser by a factor of two, based on the observed angular diameter of the optically thick dust shell. The reduced distance implies that LW Ser reached only $M_v \simeq -5.0$ at recorded maximum.

From Fig. 5 of Cohen & Rosenthal (1983) it would appear that both NQ Vul and LW Ser were subluminous at maximum. Alternatively, distances derived from the infrared blackbody angular diameter and the ejection velocity of the principal shell are underestimated.

The extinction estimate for the relatively nearby nova FH Ser is 2.8 mag which brings it close to the standard absolute-magnitude–rate-of-decline relationship. NQ Vul also would fit in well if we assume a value of $A_v = 2.5$ mag (Duerbeck 1981) based on polarization measurements, instead of 1.4 mag assumed by Cohen & Rosenthal. However, there is no evidence yet that the extinction to LW Ser is larger than 1.6 mag, whereas a value of ~ 3 mag is needed to make it appear normal at the nearer distance derived by Cohen & Rosenthal.

The velocity structure of the Hα profile suggests that the shell of LW Ser consisted of equatorial disc and polar cones. The polar axis was inclined at a small angle ($\sim 15°$) to the line of sight. However, the line profile did not give clear indication of a polar cone at the pole nearer to the earth. For reasons of symmetry, we may assume that

such a cone was indeed present, but did not contribute significantly near the peak Hα emission.

If one assumes that a nova shell is radiation-bound at least at early epochs (Ferland 1977), one would expect to see the nearer polar cone through considerable amount of neutral hydrogen. The neutral hydrogen may trap significant amount of Lα radiation resulting in an enhanced population of $n=2$ level of H. This would imply a higher amount of absorption of Hα from the nearer polar cone compared to the farther one. We are extrapolating here from the model of the shell of V1500 Cygni due to Strittmatter *et al.* (1977). In the case of V1500 Cygni ($t_3=3.6$ d), the blue peaks brightened relative to the red ones between 25–115 days from maximum (Prabhu 1977). It is possible that a similar evolution would have taken place in LW Ser after our observations had stopped, and would have shown the nearer polar cap if observations could have been extended in time.

It is unlikely that the shell of LW Ser has expanded to over 1 arcsec angular size. Though the shell cannot be resolved yet, high spectral resolution observations of different emission lines would help in constructing a more accurate model of the shell, and to ascertain whether a symmetry is apparent in the shell at the present epoch.

Acknowledgements

We thank M. V. Mekkaden for obtaining some of the Hα plates. Some of the reductions were carried out with the VAX 11/780 system at the Raman Research Institute, Bangalore. We have greatly benefited from the critical comments of L. Rosino and an anonymous referee on an earlier version of the paper. TPP acknowledges helpful discussions with H. W. Duerbeck and W. C. Seitter.

References

Andersen, P. H., Borra, E. F., Dubas, O. V. 1971, *Publ. astr. Soc. Pacific*, **83,** 5.
Andrillat, Y., Houziaux, L. 1987, *Recent Results on Cataclysmic Variables*, ESA SP-236, L985, p. 187.
Bode, M. F., Evans, A. 1983, *Mon. Not. R. astr. Soc.*, **203,** 285.
Cohen, J. G., Rosenthal, A. J. 1983, *Astrophys. J.*, **268,** 689.
Duerbeck, H. W. 1981, *Publ. astr. Soc. Pacific*, **93,** 165.
Ferland, G. J. 1977, *Nature*, **267,** 597.
Gallagher, J. S., Starrfield, S. 1978, *A. Rev. Astr. Astrophys.*, **16,** 171.
Gehrz, R. D., Grasdalen, G. L., Hackwell, J. A., Ney, E. P. 1980, *Astrophys. J.*, **237,** 855.
Herbig, J. H. 1978, *IAU Cir.* 3198.
Honda, M. 1978, *IAU Cir.* 3186.
Kozai, Y. 1978, *IAU Cir.* 3188.
McLaughlin, D. B. 1960, in *Stellar Atmospheres*, Ed. J. L. Greenstein, Univ. Chicago Press, p. 585.
Meinel, A. B., Aveni, A. F., Stockton, M. W. 1975, *Catalog of Emission Lines in Astrophysical Objects*, Tech. Rep. No. 27, Optical Science Center, Univ. Arizona, Tucson.
Mustel, E. R., Boyarchuk, A. A. 1970, *Astrophys. Space Sci.*, **6,** 183.
Prabhu, T. P. 1977, *Kodaikanal Obs. Bull., Ser. A.*, **2,** 75.
Prabhu, T. P. 1978, *IAU Cir.* 3201.
Prabhu, T. P., Anupama, G. C. 1987, *Astrophys. Space Sci.*, **131,** 479.
Prabhu, T. P., Anupama, G. C., Giridhar, S. 1987, *Bull. astr. Soc. India*, **15,** 98.

Shcherbakov, A. G. 1977, *Sov. Astr. Lett.*, **3,** 244.
Solf, J. 1983, *Astrophys. J.*, **273,** 647.
Stratton, F. J. M., Manning, W. H. 1939, *Atlas of Spectra of Nova Herculis* 1934, Solar Phys. Obs., Cambridge.
Strittmatter, P. A., Woolf, N. J., Thompson, R. I., Wilkerson, S., Angel, J. R. P., Stockman, H. S., Gilbert, G., Grandi, S. A., Larson, H., Fink, U. 1977, *Astrophys. J.*, **216,** 23.
Szkody, P., Dyck, H. M., Capps, R. W., Becklin, E. E., Cruickshank, D. P. 1979, *Astr. J.*, **84,** 1359.
van den Bergh, S., Younger, P. F. 1987, *Astr. Astrophys. Suppl. Ser.*, **70,** 125.
Weaver, H. 1974, *Highlights of Astronomy*, **3,** 509.
Yamashita, Y., Ichimura, K., Nakagiri, M., Norimoto, Y., Maehara, H., Miyajima, K. 1977, *Publ. astr. Soc. Japan*, **29,** 527.